Iran J Nucl Med. 2026;34(2):105-112 [Serial No. 67]

Homepage: https://irjnm.tums.ac.ir/

ORIGINAL RESEARCH ARTICLE

Dosimetry of [^{18}F]Fluoro-pivalic acid PET Tracer: Human dose estimates based on balb/c biodistribution data

Bahareh Bahrami Khoundabi[1], Saeed Kakaei[2], Elham Sattarzadeh Khameneh[2], Seyed Mahmoud Reza Aghamiri[1], Fariba Johari Deha[2]

[1]*Department of Medical Radiation Engineering, Faculty of Nuclear Engineering, Shahid Beheshti University, Tehran, Iran*

[2]*Radiation Application Research School, Nuclear Science and Technology Research Institute, Tehran, Iran*

ARTICLE INFO

Article History:
Received: 08 September 2025
Revised: 29 December 2025
Accepted: 12 January 2026
Published Online: 18 June 2026

Keyword:
[^{18}F]Fluoro-pivalic acid
Dosimetry
Glioma
Fatty acid metabolism
Positron emission tomography

*Corresponding Author:
Dr. Saeed Kakaei
Address: Radiation Application Research School, Nuclear Science and Technology Research Institute, P. O. Box 11365-3486, Tehran, Iran.
Email: skakaei@aeoi.org.ir

ABSTRACT

Introduction: [^{18}F]Fluoro-pivalic acid ([^{18}F]FPIA) is a PET radiotracer under investigation for imaging short-chain fatty acid (SCFA) metabolism in gliomas. Accurate human radiation dosimetry is a prerequisite for its clinical translation. This study aimed to estimate human organ absorbed doses of [^{18}F]FPIA based on biodistribution data obtained from normal BALB/c mice.

Methods: [^{18}F]FPIA was synthesized at the Karaj Cyclotron Center (Karaj, Iran) via nucleophilic fluorination of a tosyl precursor. For biodistribution studies, female BALB/c mice (n=3 per time point, total n=9) were intravenously injected with 0.526 mCi (19.46 MBq). Animals were sacrificed at 15, 30, and 60 minutes post-injection. Radioactivity in major organs was measured using a well-type NaI(Tl) detector and expressed as percentage of injected dose per gram (%ID/g). Time-activity curves were generated via trapezoidal integration and exponential fitting. Cumulative organ activities were calculated and extrapolated to humans using the Sparks–Aydogan mass scaling method. Human organ absorbed doses and the effective dose were estimated using the Medical Internal Radiation Dose (MIRD) formalism implemented in OLINDA/EXM 2.0 software.

Results: The highest estimated absorbed doses in human organs were observed in the bladder wall (0.201 mGy/MBq) and kidneys (0.143 mGy/MBq). In contrast, the brain (0.0274 mGy/MBq) and intestines (0.0196 mGy/MBq) received the lowest doses. The estimated effective dose was 0.016 mSv/MBq.

Conclusion: The dosimetry profile of [^{18}F]FPIA, characterized by low background brain exposure and favorable dose estimates comparable to other clinical ^{18}F-tracers, supports its safe application for PET imaging. These results facilitate the clinical translation of [^{18}F]FPIA for tracing SCFA metabolism in glioma studies.

Use your device to scan and read the article online

How to cite this article: Bahrami Khoundabi B, Kakaei S, Sattarzadeh Khameneh E, Aghamiri SMR, Johari Deha F. Dosimetry of [^{18}F]Fluoro-pivalic acid PET Tracer: Human dose estimates based on balb/c biodistribution data. Iran J Nucl Med. 2026;34(2):105-112.

https://doi.org/10.22034/irjnm.2026.130296.1707

INTRODUCTION

Gliomas represent the most prevalent and aggressive category of primary brain tumors, constituting nearly 80% of all primary central nervous system (CNS) malignancies [1]. Glioblastoma (GBM), the most common and lethal subtype, has a dismal prognosis with a median survival of approximately 12-15 months despite multimodal therapy [2, 3]. Early detection and precise molecular characterization are therefore critical for improving patient management. Positron emission tomography (PET) with metabolic radiotracers offers a powerful, non-invasive tool for evaluating tumor biology and profiling [4]. Altered cellular metabolism is a hallmark of cancer. Gliomas exhibit not only enhanced glycolysis (Warburg effect) but also upregulated de novo fatty acid synthesis to support rapid membrane biogenesis and proliferation [5, 6]. Consequently, radiotracers targeting short-chain fatty acid (SCFA) metabolism, such as [^{11}C]acetate and [^{18}F]fluoroacetate (FAC), have been explored for glioma imaging [7, 8]. While ^{18}F-fluorodeoxyglucose ([^{18}F]FDG) is the most widely used PET tracer in oncology, its high physiological uptake in normal gray matter significantly limits contrast and utility in brain tumor imaging [9]. [^{18}F]Fluoro-pivalic acid ([^{18}F]FPIA), a branched-chain SCFA analog, has emerged as a promising alternative. Preclinical studies indicate that [^{18}F]FPIA exhibits low retention in normal brain tissue while demonstrating significant uptake in glioma models, leading to superior tumor-to-brain contrast ratios compared to [^{18}F]FDG [10, 11]. This property is attributed to the preferential utilization of fatty acids by glioma cells for energy production and biosynthesis [12, 13]. The initial promise of [^{18}F]FPIA warrants its progression toward clinical evaluation. A mandatory step in the clinical translation of any novel radiopharmaceutical is the assessment of human radiation exposure through internal dosimetry. Regulatory agencies require human dose estimates, typically derived from preclinical biodistribution data, to ensure patient safety and define administered activity limits [14-16]. The Medical Internal Radiation Dose (MIRD) formalism, combined with species scaling methods like that of Sparks and Aydogan, provides a validated framework for this extrapolation [17-19]. While prior studies have demonstrated the imaging efficacy of [^{18}F]FPIA in preclinical models [10, 11, 20], comprehensive human radiation dose estimates based on standardized methodologies are lacking. This study aimed to address this critical gap. We report the synthesis, quality control, and biodistribution of [^{18}F]FPIA in normal BALB/c mice. Subsequently, we employed the MIRD methodology with Sparks-Aydogan scaling to provide the first estimated human organ absorbed doses for [^{18}F]FPIA, thereby facilitating its safe introduction into clinical trials for glioma imaging.

METHODS

Chemicals and reagents

All chemicals, including 4-dimethylaminopyridine (DMAP), 4-toluenesulfonyl chloride (TsCl), pyridine, Kryptofix 2.2.2 (K222), and all solvents, were of analytical grade and purchased from Sigma-Aldrich (MO, USA), Merck, or Fluka. The non-radioactive precursor, methyl 2, 2-dimethyl-3-hydroxypropionate, was obtained from Chem Cruz®. Enriched [^{18}O]H_2O (97–98% isotopic purity) was used for the production of no-carrier-added [^{18}F]fluoride ion.

Preparation and quality control of [18F]FPIA

The radiosynthesis of [^{18}F]FPIA was performed using a modified procedure based on previously published methods [21-23], as summarized in Figure 1.

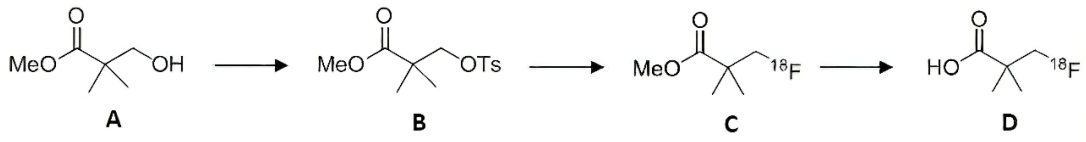

Figure 1. Synthesis and hydrolysis steps for [^{18}F]fluoro pivalic acid. A: methyl 2, 2-dimethyl-3-hydroxypropionate, B: Methyl2, 2-dimethyl-3-[(4-methylbenzenesulfonyl) oxy] propanoate, C: Labelled product, D: [^{18}F] FPIA radiopharmaceutical

Synthesis of the Tosyl precursor: The non-radioactive precursor, methyl 2, 2-dimethyl-3-[(4-methylbenzenesulfonyl)oxy]propanoate, was synthesized from methyl 2,2-dimethyl-3-hydroxypropionate. Briefly, the starting material (200 µL) and 4-dimethylaminopyridine (DMAP, 9.2 mg) were dissolved in anhydrous pyridine (0.5 mL). A solution of 4-toluenesulfonyl chloride (TsCl, 347 mg) in pyridine (2 mL) was added dropwise. The reaction mixture was stirred at room temperature under a nitrogen atmosphere for 3 hours. The mixture was then diluted with dichloromethane (DCM) and washed sequentially with water, 1M HCl, and brine. The organic layer was dried over anhydrous Na_2SO_4,

filtered, and concentrated under reduced pressure. The resulting residue was purified by flash column chromatography (15% ethyl acetate in petroleum ether) to yield the pure tosyl precursor as a white solid. The identity and purity of the compound were confirmed by ^{1}H-NMR spectroscopy (Bruker DRX 300 MHz).

M.p: 83-85 ˚C: ^{1}HNMR (400 MHz, $CDCl_3$) δ: 7.71 (d, J = 8.3 Hz, 2H; Ar), 7.26 (d, J = 8.0 Hz, 2H; Ar), 4.03 (s, 2H; 3-H), 3.53 (s, 3H; OMe), 2.38 (s, 3H; Ph-Me), 1.11 (s, 6H; CH_3-2).

Radiosynthesis: No-carrier-added [^{18}F]fluoride was produced via the ^{18}O(p,n) ^{18}F nuclear reaction by irradiating [^{18}O]H_2O with 18-MeV protons on a KIUBE-180 cyclotron (IBA). The automated radiolabeling was performed on an IBA Synthera® module. The aqueous [^{18}F]fluoride solution was trapped on a QMA carbonate light cartridge, eluted with a solution of Kryptofix® 222 (K_2.2.2, 15 mg) and K_2CO_3 (3 mg) in acetonitrile/water (80:20 v/v), and dried azeotropically at 110°C under a stream of nitrogen. The dried [^{18}F]fluoride-K_2.2.2 complex was reacted with the tosyl precursor (5-10 mg) in anhydrous acetonitrile (1 mL) at 60°C for 10 minutes. The intermediate [^{18}F]fluoro-ester was then hydrolyzed by the addition of 1M NaOH (0.5 mL) and heating at 60°C for 5 minutes. The reaction was quenched and neutralized with 1M HCl (0.5 mL).

Purification and formulation: The crude reaction mixture was purified by semi-preparative reverse-phase HPLC on a Phenomenex Luna C18 column (250 x 10 mm, 5 µm) using an isocratic mobile phase of acetonitrile: water: acetic acid (50:50:0.1, v/v/v) at a flow rate of 4 mL/min. The fraction corresponding to [^{18}F]FPIA (retention time ~ 8-9 min) was collected, diluted with sterile water, and passed through a C_{18} Sep-Pak® light cartridge. The product was eluted with ethanol (1 mL), diluted with sterile physiological saline (9 mL), and passed through a 0.22 µm sterile filter into a sterile, pyrogen-free vial.

Quality control and radiochemical data: The decay-corrected radiochemical yield (RCY) was 30 ± 5% (n > 10 syntheses), with a total synthesis time of 55 ± 5 minutes. Radiochemical purity (RCP) was determined by analytical radio-thin-layer chromatography (radio-TLC) on silica gel plates using acetonitrile: water (95:5, v/v) as the mobile phase, and analyzed using a MiniGita radio-TLC scanner (Raytest, Germany). Under these conditions, [^{18}F]FPIA migrates with the solvent front (R_f = 0.8–0.9), while free [^{18}F]fluoride remains at the origin (R_f = 0.0–0.1). Identity was confirmed by co-injection with an authentic non-radioactive pivalic acid standard using analytical HPLC. The RCP at end-of-synthesis (EOS) consistently exceeded 99%. The pH of the final formulation was 5.5–7.5. Sterility and apyrogenicity tests were performed according to pharmacopeial standards. The final product was obtained as a sterile, isotonic solution suitable for intravenous injection.

Biodistribution of [^{18}F]FPIA in normal mice

All animal experiments were conducted in compliance with the institutional guidelines for the care and use of laboratory animals and were approved by the relevant ethics committee. The pharmacokinetics and tissue distribution of [^{18}F]FPIA were evaluated in healthy female BALB/c mice (n=3 per time point). Female BALB/c mice (age: 6–8 weeks; weight: 18–22 g) were used for the study. Animals received an intravenous injection of 0.526 mCi (19.46 MBq) via the tail vein. At 15, 30, and 60 minutes post-injection, mice were euthanized, and organs were collected, weighed, and counted using a calibrated NaI(Tl) well counter. Counts were corrected for background, efficiency, and decay-corrected back to the time of injection.

Tracer uptake was quantified using two standard metrics including percentage of injected dose per gram of tissue (%ID/g) and standardized uptake value (SUV). All biodistribution data are presented as decay-corrected mean %ID/g ± SD (Table 1).

Table 1. The Percentage of injected activity per gram (%ID/g) of [^{18}F]FPIA in normal mice

Organ	Time		
	15 min	30 min	60 min
Liver	22.70±6.41	7.19±0.10	4.45±0.14
Kidney	20.29±2.80	9.84±1.043	6.38±0.09
Bladder	13.98±21.69	62.21±47.50	27.03±41.99
Blood	13.55±6.91	4.64±0.42	4.39±0.59
Lung	7.81±3.52	3.44±0.74	3.02±0.32
Heart	7.55±4.81	3.45±0.35	3.40±0.38
Stomach	4.37±2.52	2.36±0.69	2.50±1.59
Intestine	3.82±2.29	2.08±0.36	2.04±0.004
Spleen	3.56±1.67	2.34±0.23	1.75±0.11
Bone	3.21±1.10	2.77±0.36	3.47±0.61
Brain	1.14±0.46	1.00±0.10	1.10±0.06

Biodistribution measurements and analysis: The radioactivity in each tissue sample was measured using a well-type NaI(Tl)scintillation detector (Gamma Surveyor, S.E. International, Inc.). A symmetric energy window of 450–550 keV was set around the 511 keV annihilation peak to optimize counting efficiency and minimize background. The detector was calibrated weekly for energy and efficiency using a ^{137}Cs standard source. The system's absolute counting efficiency for 511 keV photons under these conditions was 68%. All measured counts were automatically corrected for background, physical decay (of ^{18}F), and detector efficiency using the instrument's software.

Software and data analysis: Biodistribution data were processed, and time-activity curves (TACs) were generated using GraphPad Prism software (Version 9.0, GraphPad Software, USA). TACs were constructed by plotting decay-corrected mean %ID/g versus time. For most organs exhibiting clearance (e.g., blood, liver), data points were fitted with a bi-exponential function. For the bladder, which showed accumulation, trapezoidal integration was applied from t=0 to the last data point (60 min). Cumulative activities for each source organ were calculated by integration of the time-activity curves from time zero to infinity, assuming physical decay beyond the last measured time point. Human organ absorbed doses and the effective dose were calculated using the Medical Internal Radiation Dose (MIRD) formalism as implemented in the OLINDA/EXM 2.0 software (Vanderbilt University, USA). The software's adult male phantom and ICRP Publication 103 tissue weighting factors were used for the final effective dose calculation.

Pharmacokinetic modeling and human dosimetry estimation

Generation of time-activity curves (TACs) and cumulated activity (Ã): The measured radioactivity in each tissue was expressed as the percentage of the injected dose per gram of tissue(%ID/g) [24]. The activity concentration, Ac (t), at a given time point t was calculated as:

$$Ac(t) = (A_{tissue}(t) / M_{tissue}(t)) / A_{total} \times 100\%$$

where Atissue(t) is the activity (MBq) in the tissue sample, Mtissue (t) is the mass (g) of the tissue, and Atotal is the total injected activity (MBq) [25].

Decay-corrected mean %ID/g values for each organ were plotted versus time. Time-Activity Curves (TACs) were generated by fitting the data points. $\widetilde{A_{r_s}} = \int_0^\infty A(t)dt$ where $\widetilde{A_{r_s}}$ (t) is the activity in source organ r_s at time t [26]. The cumulative activity for each organ in mice was estimated by plotting the mean %ID/g values versus time, connecting the data points, and calculating the area under the curve (AUC) from time zero to infinity using the trapezoidal integration method. For time points beyond the last measurement (60 min), the clearance was assumed to follow the physical decay of ^{18}F (T{1/2} = 109.8 min).

Extrapolation to humans using the Sparks–Aydogan Model: The Sparks–Aydogan relative organ mass-scaling method was selected to extrapolate murine Ã to human values [27, 28]. This method is a standardized approach for early-phase biodistribution data, assuming the fraction of total body activity in an organ scales with its fractional body mass. We acknowledge its limitation in not accounting for potential interspecies differences in metabolism or excretion rates. The human cumulated activity ($\tilde{A}_{human}$) was calculated as:

$$\tilde{A}_{human} = \tilde{A}_{mouse} \times (M_{human\text{-}organ} / M_{mouse\text{-}organ}) \times (M_{mouse\text{-}total} / M_{human\text{-}total})$$

Standard organ/body masses for a 73.7 kg adult male (ICRP 89) and a 0.02 kg mouse were used.

Absorbed dose calculation: The mean absorbed dose $D(r_T)$ to each target organ (r_t) was calculated using the Medical Internal Radiation Dosimetry (MIRD) formalism [27, 29]:

$$D(r_T) = \sum_{r_s} \tilde{A}_{r_s} S(r_t \leftarrow r_s)$$

where S ($r_t \leftarrow r_s$) is the S-value, representing the mean absorbed dose to target organ (r_t) per unit cumulative activity in source organ (r_s) [15, 30]. Where S-values for ^{18}F were obtained from the OLINDA/EXM 2.0 software (adult male phantom. The dynamic bladder model (voiding interval: 3.5 h) was used for the bladder wall dose. The effective dose was calculated using ICRP 103 tissue weighting factors.

RESULTS

Biodistribution and Pharmacokinetics

The decay-corrected biodistribution data are presented in Table 1. [^{18}F]FPIA showed rapid blood clearance and prominent hepatorenal excretion. Liver uptake was highest at 15 min (22.70 ± 6.41 %ID/g), declining thereafter. Kidney uptake was moderate (20.29 ± 2.80 %ID/g at 15 min). Bladder content was highly variable (e.g., 62.2 ± 47.5 %ID/g at 30 min), reflecting differences in individual diuresis under anesthesia; this variability is propagated into the uncertainty of the bladder wall dose estimate. Brain uptake was low and stable across time points (~1.1 %ID/g), confirming minimal retention in normal brain parenchyma.

Human radiation dose estimates

The estimated human absorbed doses are listed in Table 2. As expected for a renally cleared tracer, the highest doses were received by the urinary bladder wall (0.201 mGy/MBq) and kidneys (0.143 mGy/MBq). The effective dose was 0.016 mSv/MBq. For a standard 370 MBq administration, this an effective dose, comparable to other diagnostic ^{18}F-tracers (Table 3).

Table 2. Estimation of absorbed dose by MIRD method in human body for ^{18}F-FPIA

Organs	Absorbed dose (mGy/MBq)
Kidney	1.43E-01
Bladder	2.01E-01
Spleen	1.04E-01
Lung	1.37E-01
Heart	4.14E-02
Brain	2.74E-02
Bone	6.02E-02
Liver	4.93E-02
Stomach	3.44E-02
Intestine	1.96E-02

DISCUSSION

We report an improved radio synthesis of [^{18}F]FPIA (RCY: 30%), facilitating reliable production. The murine biodistribution aligns with prior studies, showing rapid clearance and low brain uptake. The observed ~1 %ID/g in brain, while low relative to abdominal organs, is notable. For a short-chain fatty acid analog, this may indicate specific, low-capacity transport across the blood-brain barrier or represent a non-specific background. This level is significantly lower than that of [^{18}F-FDG] but should be considered when evaluating its absolute specificity.

A recent first-in-human study of [^{18}F]FPIA has been published [23]. Our mouse-derived effective dose estimate (0.016 mSv/MBq) is in good agreement with the clinically measured value from that study (0.015 mSv/MBq), validating our preclinical dosimetry approach. Furthermore, the human PET data confirmed the low physiological brain uptake and high tumor-to-brain contrast we predicted, strengthening the rationale for its neuro-oncological application.

In current study, we employed the Sparks–Aydogan scaling method for its practicality with biodistribution data, while acknowledging that methods like allometric scaling or direct PET-based human measurements are more accurate. The high variability in bladder activity is a study limitation, common in rodent biodistribution studies due to physiological variability under anesthesia; we addressed this using a standardized physiological model in OLINDA/EXM. The primary goal of this preclinical dosimetry was to provide a safety estimate to support regulatory approval for initial clinical trials, which has been achieved.

Table 3. Comparison of effective dose (mSv/MBq) and critical organ doses (mGy/MBq) for selected ^{18}F-labeled PET tracers

Tracer	Effective Dose	Critical Organ Dose	Primary Excretion	Reference
[^{18}F]FPIA	0.016	Bladder Wall (0.201)	Renal/Hepatic	This work
[^{18}F]FDG	0.019	Bladder Wall (0.13)	Renal	ICRP 128
[^{18}F]FET	0.022	Urinary Bladder (0.18)	Renal	[21]
[^{18}F]FLT	0.027	Bladder Wall (0.21)	Renal	[22]

Figure 2 summarizes the workflow including radiotracer synthesis, mouse biodistribution, TAC fitting & Ã calculation, mass-scaling, and human dose estimation via MIRD/OLINDA.

This study successfully addresses a crucial prerequisite for the clinical translation of the novel PET tracer[^{18}F]FPIA by establishing a reproducible synthesis method and providing its first comprehensive preclinical radiation dosimetry profile, based on biodistribution data from healthy mice. The work was conducted at the Karaj Cyclotron Center, Iran, using a standardized methodology. Our radiosynthesis of [^{18}F]FPIA was optimized to achieve a decay-corrected radiochemical yield of 30%, which represents a substantial improvement over previously reported yields of 11.3 ± 4.1% , 7.7 ± 5.0% and 19.4 ± 1.9% [21- 23]. This enhancement in yield, coupled with a synthesis time under 60 minutes and a consistent radiochemical purity exceeding 99%, defines a reliable production process suitable for future clinical application. The biodistribution profile of [^{18}F]FPIA in healthy BALB/c mice aligns with and extends previous findings. Consistent with reports by Witney et al. and Dubash et al. [22, 23], we observed very low and stable uptake in normal brain tissue (average ~1.1 %ID/g from 15-60 min). This minimal background retention is the tracer's most critical attribute for neuro-oncology, as it promises high tumor-to-brain contrast—a key advantage over [^{18}F]FDG, whose high physiological brain uptake limits its utility for glioma imaging [9]. This low baseline confirms that [^{18}F]FPIA crosses the intact blood-brain barrier, a prerequisite for targeting intracranial tumors. The uptake value, while low, is measurable and should be interpreted in the context of specific tumor targeting versus non-specific background. The tracer exhibited rapid blood clearance and prominent uptake in excretory organs. High initial accumulation in the kidneys and liver, followed by significant and variable activity in the bladder, indicates a primary clearance pathway

via renal excretion with a complementary hepatobiliary component, as previously suggested by PET imaging studies [22]. The high standard deviation in bladder activity (Table 1) underscores the physiological variability in urine excretion under experimental conditions, a common challenge in rodent biodistribution that we accounted for using a standardized model in OLINDA. This pattern is characteristic of small, polar metabolites and results in low off-target retention in organs such as the heart, lungs, and spleen. The extrapolation of murine biodistribution data to humans using the standardized MIRD formalism and Sparks-Aydogan mass scaling yielded absorbed dose estimates that support the tracer's safe use. We selected the Sparks-Aydogan method as it provides a straightforward, conservative scaling factor based on organ mass ratios, widely accepted for preliminary dose estimation from rodent data [28]. As anticipated for a renally cleared agent, the calculated doses were highest for the urinary bladder wall (0.201 mGy/MBq) and kidneys (0.143 mGy/MBq). The estimated effective dose was approximately 0.016 mSv/MBq. To contextualize this dosimetry, Table 3 compares [18F]FPIA with other common 18F-labeled clinical tracers. Its effective dose and critical organ doses are highly comparable to those of established tracers like 18F-fluoroethyltyrosine (FET) and 18F-fluorothymidine (FLT). An administration of 370 MBq would result in an effective dose, which is within the standard range for diagnostic PET and poses no exceptional radiation risk. Notably, our preclinical estimates show strong concordance with the first-in-human dosimetry results recently published by Dubash et al. [23], where the measured effective dose was 0.016 mSv/MBq. This agreement validates the methodological approach used in this study and increases confidence in the reliability of the dose estimates presented here. These favorable safety data are particularly significant given the promising imaging efficacy demonstrated preclinically. In U87 glioma models, [18F]FPIA showed tumor uptake comparable to [18F]FDG but achieved a significantly superior tumor-to-brain ratio (2.5 vs. 1.3) due to its low brain background [22]. This high contrast is essential for reliably detecting and delineating gliomas.

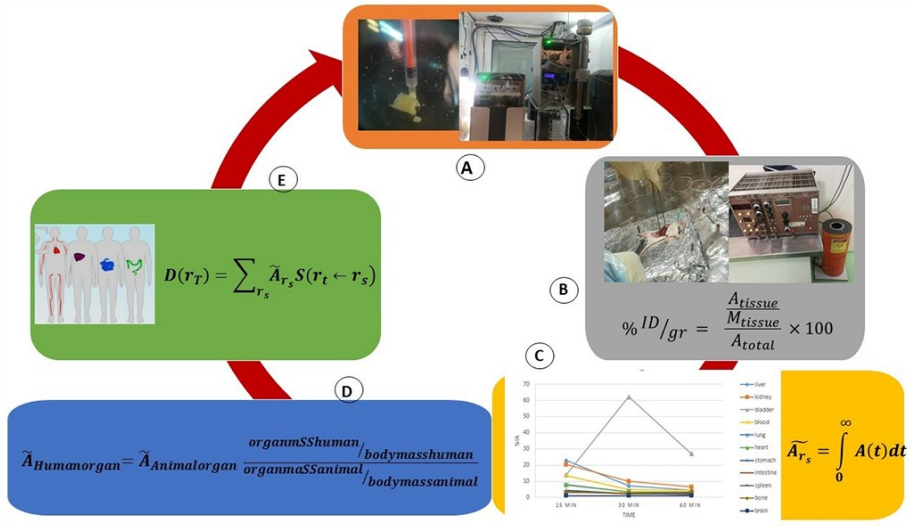

Figure 2. Schematic workflow. A: Radiosynthesis of [18F]FPIA, B: Animal biodistribution, C: Time–activity curve generation and estimation of cumulated activity, D: The Sparks-Aydogan scaling, E: Human absorbed dose estimation

Limitations and future directions

The primary limitation of this work is inherent to all preclinical dosimetry:the estimates are derived from animal data and scaled to human anatomy, which may not fully capture interspecies differences in tracer kinetics. The high variability in bladder activity, although addressed using a standardized physiological model, also introduces some uncertainty. Additionally, the assumed bi-exponential clearance for some organs and the use of mass-scaling without metabolic correction are simplifications. Therefore, these dose estimates should be considered preliminary. The logical next step is a Phase I clinical trial to validate human biodistribution and dosimetry via direct PET imaging. Subsequent studies should evaluate the diagnostic performance of [18F]FPIA in patients with primary and recurrent glioma, comparing its accuracy directly with [18F]FDG and amino acid tracers like [18F]FET.

CONCLUSION

This study successfully synthesized the novel PET tracer [^{18}F]FPIA with an improved radiochemical yield and characterized its pharmacokinetics and radiation dosimetry as a critical step toward clinical translation. The key findings are threefold. First, the optimized radiosynthesis provided a reliable supply of the tracer with high purity. Second, biodistribution studies in healthy mice confirmed an ideal profile for brain imaging: rapid systemic clearance, prominent renal excretion, and, most importantly, persistently low uptake in normal brain tissue, which is essential for achieving high tumor-to-background contrast. Third, extrapolation to human models using established MIRD methodology yielded a favorable dosimetry profile. The estimated effective dose of approximately 0.016 mSv/MBq is comparable to those of other widely used ^{18}F-labeled diagnostic tracers, with the urinary bladder wall and kidneys identified as the critical organs. These preclinical estimates are further supported by their agreement with recently published clinical data. Collectively, the low background brain exposure and acceptable radiation safety profile strongly support the transition of [^{18}F]FPIA into initial clinical trials. These results provide the necessary preclinical foundation to evaluate its efficacy in PET imaging of fatty acid metabolism in patients with glioma, where it holds significant promise for improving tumor detection and characterization.

Acknowledgements

The authors gratefully acknowledge the technical support and collaboration of the staff at the Karaj Cyclotron Center, Nuclear Science and Technology Research Institute (NSTRI). We specifically thank the Radiation Application Research School for providing the necessary laboratory facilities and resources. This work was supported by the NSTRI. We also extend our appreciation to our colleagues in the radiochemistry and animal facility units for their expert assistance.

REFERENCES

1. Lin S, Xu H, Zhang A, Ni Y, Xu Y, Meng T, Wang M, Lou M. Prognosis analysis and validation of m6A signature and tumor immune microenvironment in glioma. Front Oncol. 2020 Oct 5;10:541401.
2. Dolecek TA, Propp JM, Stroup NE, Kruchko C. CBTRUS statistical report: primary brain and central nervous system tumors diagnosed in the United States in 2005-2009. Neuro Oncol. 2012 Nov;14 Suppl 5(Suppl 5):v1-49.
3. Omuro A, DeAngelis LM. Glioblastoma and other malignant gliomas: a clinical review. JAMA. 2013 Nov 6;310(17):1842-50.
4. Ostrom QT, Gittleman H, Xu J, Kromer C, Wolinsky Y, Kruchko C, Barnholtz-Sloan JS. CBTRUS statistical report: primary brain and other central nervous system tumors diagnosed in the United States in 2009–2013. Neuro Oncol. 2016 Oct 1;18(suppl_5):v1-v75.
5. Overcast WB, Davis KM, Ho CY, Hutchins GD, Green MA, Graner BD, Veronesi MC. Advanced imaging techniques for neuro-oncologic tumor diagnosis, with an emphasis on PET-MRI imaging of malignant brain tumors. Curr Oncol Rep. 2021 Feb 18;23(3):34.
6. Baenke F, Peck B, Miess H, Schulze A. Hooked on fat: the role of lipid synthesis in cancer metabolism and tumour development. Dis Model Mech. 2013 Nov;6(6):1353-63.
7. Oyama N, Akino H, Kanamaru H, Suzuki Y, Muramoto S, Yonekura Y, Sadato N, Yamamoto K, Okada K. 11C-acetate PET imaging of prostate cancer. J Nucl Med. 2002 Feb;43(2):181-6.
8. Ponde DE, Dence CS, Oyama N, Kim J, Tai YC, Laforest R, Siegel BA, Welch MJ. 18F-fluoroacetate: a potential acetate analog for prostate tumor imaging--in vivo evaluation of 18F-fluoroacetate versus 11C-acetate. J Nucl Med. 2007 Mar;48(3):420-8.
9. Witney TH, Alam IS, Turton DR, Smith G, Carroll L, Brickute D, Twyman FJ, Nguyen QD, Tomasi G, Awais RO, Aboagye EO. Evaluation of deuterated 18F- and 11C-labeled choline analogs for cancer detection by positron emission tomography. Clin Cancer Res. 2012 Feb 15;18(4):1063-72.
10. Clark PM, Mai WX, Cloughesy TF, Nathanson DA. Emerging approaches for targeting metabolic vulnerabilities in malignant glioma. Curr Neurol Neurosci Rep. 2016 Feb;16(2):17.
11. Lin H, Patel S, Affleck VS, Wilson I, Turnbull DM, Joshi AR, Maxwell R, Stoll EA. Fatty acid oxidation is required for the respiration and proliferation of malignant glioma cells. Neuro Oncol. 2017 Jan;19(1):43-54.
12. Pike LS, Smift AL, Croteau NJ, Ferrick DA, Wu M. Inhibition of fatty acid oxidation by etomoxir impairs NADPH production and increases reactive oxygen species resulting in ATP depletion and cell death in human glioblastoma cells. Biochim Biophys Acta. 2011 Jun;1807(6):726-34.
13. Verger A, Kas A, Darcourt J, Guedj E. PET imaging in neuro-oncology: An update and overview of a rapidly growing area. Cancers. 2022 Feb 22;14(5):1103.
14. Mashimo T, Pichumani K, Vemireddy V, Hatanpaa KJ, Singh DK, Sirasanagandla S, Nannepaga S, Piccirillo SG, Kovacs Z, Foong C, Huang Z, Barnett S, Mickey BE, DeBerardinis RJ, Tu BP, Maher EA, Bachoo RM. Acetate is a bioenergetic substrate for human glioblastoma and brain metastases. Cell. 2014 Dec 18;159(7):1603-14.
15. Snyder WS, Ford MR, Warner GG, Watson S. MIRD pamphlet no. 11: S, absorbed dose per unit cumulated activity for selected radionuclides and organs. New York: Society of Nuclear Medicine. 1975.
16. Shanehsazzadeh S, Lahooti A, Yousefnia H, Geramifar P, Jalilian AR. Comparison of estimated human dose of (68)Ga-MAA with (99m)Tc-MAA based on rat data. Ann Nucl Med. 2015 Oct;29(8):745-53.
17. Hu LS, Hawkins-Daarud A, Wang L, Li J, Swanson KR. Imaging of intratumoral heterogeneity in high-grade glioma. Cancer Lett. 2020 May 1;477:97-106. doi: 10.1016/j.canlet.2020.02.025. Epub 2020 Feb 27. PMID: 32112907; PMCID: PMC7108976.
18. Albert NL, Weller M, Suchorska B, Galldiks N, Soffietti R, Kim MM, la Fougère C, Pope W, Law I, Arbizu J, Chamberlain MC, Vogelbaum M, Ellingson BM, Tonn JC. Response assessment in neuro-oncology working group and European association for neuro-oncology recommendations for the clinical use of PET imaging in gliomas. Neuro Oncol. 2016 Sep;18(9):1199-208.

19. Mohammadi BM, Shirmardi SP, Shokri AA, Erfani M. Estimation of organ-absorbed doses in human from gamma rays of 99mTc-DTPA radiopharmaceutical, using the animal dissection data. Arch Adv Biosci. 2019 Nov 26;10(4):22-30.
20. Vassileva V, Braga M, Barnes C, Przystal J, Ashek A, Allott L, Brickute D, Abrahams J, Suwan K, Carcaboso AM, Hajitou A. Effective detection and monitoring of glioma using [18F] FPIA PET imaging. Biomedicines. 2021 Jul 13;9(7):811.
21. Pisaneschi F, Witney TH, Iddon L, Aboagye EO. Synthesis of [18 F] fluoro-pivalic acid: an improved PET imaging probe for the fatty acid synthesis pathway in tumours. Med chem comm. 2013;4(10):1350-3.
22. Witney TH, Pisaneschi F, Alam IS, Trousil S, Kaliszczak M, Twyman F, Brickute D, Nguyen QD, Schug Z, Gottlieb E, Aboagye EO. Preclinical evaluation of 3-18F-fluoro-2,2-dimethylpropionic acid as an imaging agent for tumor detection. J Nucl Med. 2014 Sep;55(9):1506-12.
23. Dubash SR, Keat N, Kozlowski K, Barnes C, Allott L, Brickute D, Hill S, Huiban M, Barwick TD, Kenny L, Aboagye EO. Clinical translation of 18F-fluoropivalate - a PET tracer for imaging short-chain fatty acid metabolism: safety, biodistribution, and dosimetry in fed and fasted healthy volunteers. Eur J Nucl Med Mol Imaging. 2020 Oct;47(11):2549-61.
24. Shanehsazzadeh S, Gruettner C, Lahooti A, Mahmoudi M, Allen BJ, Ghavami M, Daha FJ, Oghabian MA. Monoclonal antibody conjugated magnetic nanoparticles could target MUC-1-positive cells in vitro but not in vivo. Contrast Media Mol Imaging. 2015 May-Jun;10(3):225-36.
25. Jalilian AR, Shanehsazzadeh S, Akhlaghi M, Garousi J, Rajabifar S, Tavakoli MB. Preparation and biodistribution of [Ga-67]-DTPA-gonadorelin in normal rats. J Radioanal Nucl Chem.2008;278(1):123-9.
26. Bolch WE, Eckerman KF, Sgouros G, Thomas SR. MIRD pamphlet No. 21: a generalized schema for radiopharmaceutical dosimetry--standardization of nomenclature. J Nucl Med. 2009 Mar;50(3):477-84.
27. Khorrami Moghaddam A, Reza Jalilian A, Hayati V, Shanehsazzadeh S. Determination of human absorbed dose of 201Tl(III)-DTPA-HIgG based on biodistribution data in rats. Radiat Prot Dosimetry. 2010 Oct;141(3):269-74.
28. Sparks RB, Aydogan B. Comparison of the effectiveness of some common animal data scaling techniques in estimating human radiation dose. Oak Ridge Associated Universities, 1999 Jan 1; TN, United States.
29. Bevelacqua JJ. Internal dosimetry primer. Radiat Prot Manag. 2005 Jan 1;22(5):7.
30. Xie T, Lee C, Bolch WE, Zaidi H. Assessment of radiation dose in nuclear cardiovascular imaging using realistic computational models. Med Phys. 2015 Jun;42(6):2955-66.